J Mater Sci (2023) 58:707–717

Ceramics

Correlation between microstructure and mechanical properties of ZTA–TiO_2–Nb_2O_5 ceramics sintered by SPS

Yudong Sui[1,2], Yanru Yuan[1,2], Pan Tan[1,2], Yehua Jiang[1,2,*], and Lina Han[1]

[1] School of Materials Science and Engineering, Kunming University of Science and Technology, 253, Xuefu Road, Kunming 650093, People's Republic of China

[2] National and Local Joint Engineering Laboratory of Advanced Metal Solidification Forming and Equipment Technology, Kunming University of Science and Technology, Kunming 650093, People's Republic of China

Received: 20 September 2022
Accepted: 20 December 2022
Published online: 1 January 2023

ABSTRACT

This paper presents the experimental investigation of the effect of Nb_2O_5 content on the phase composition, microstructure, and physical and mechanical performance of the zirconia-toughened alumina (ZTA) ceramics, aimed to optimize the additional amount of Nb_2O_5, refine the ceramic grains, and improve the densification, hardness and fracture toughness. ZTA ceramics with various Nb_2O_5 contents were prepared using the spark plasma sintering method. The addition of trace amounts of Nb_2O_5 did not produce a new Nb-rich phase; the Nb atoms were dissolved in the ZrO_2 grains. The addition of trace amounts of Nb_2O_5 led to grain refinement and an increase in density, but the addition of excessive Nb_2O_5 resulted in grain growth and a decrease in relative density. Furthermore, the addition of Nb_2O_5 promoted uniformity of the microstructure. The sample with 0.25 wt.% Nb_2O_5 had the maximum Vickers hardness and indentation fracture toughness, which were 1228.40 HV and 9.17 MPa $\sqrt{m}$, respectively. Mechanical properties of the composite mainly depended on the grain size, which was influenced to some extent by the relative density.

Introduction

Zirconia-toughened alumina (ZTA) ceramics are used as structural and functional materials (for example, ceramic sleeves, cutting blades, biomedical implants, and piezoelectric ceramics) because of their outstanding physical and mechanical properties [1–3]. Although ZTA ceramics have better fracture toughness and higher hardness than Al_2O_3 and ZrO_2, respectively, it still below the standardised requirement for the aforementioned applications [4].

Handling Editor: David Cann.

Address correspondence to E-mail: jiangyehua@kmust.edu.cn

https://doi.org/10.1007/s10853-022-08114-7

Methods to improve the toughness of ZTA composites include the addition of a stabiliser and a sintering agent to improve the toughness via phase transformation toughening and microstructure refinement and the use of non-traditional processing techniques to refine the microstructure, increase the density, and improve the toughness.

The main toughening mechanism of ZTA composites is the t–m transformation of the ZrO_2 phase. When ZTA ceramics are subjected to stress, the stress-induced metastable t-ZrO_2 phase transforms into the m-ZrO_2 phase [5, 6]. TiO_2, MgO, CeO_2, and other stabilisers have been used to improve the stability and enhance the t–m transformation toughening ability of the t-ZrO_2 phase [7–9]. As an excellent stabiliser, the addition of 3 wt.% TiO_2 to ZTA composites results in finer grains, higher density, and excellent performance (1616 HV vs. 1516 HV for pure ZTA) [10, 11]. On this basis, RE_2O_3 was added to improve the toughness of ZTA ceramics by affecting the t-ZrO_2 transformation toughening mechanism [12]. Xia et al. [13] reported that Cr_2O_3 and Cr_2O_3 derived from $Cr(NO_3)_3{\cdot}9H_2O$ can significantly enhance the densification of ZTA ceramics by forming solid solutions with Al_2O_3 and ZrO_2. Sui et al. [14] reported that the addition of 3 wt.% Ta_2O_5 can refine the ZrO_2 and Al_2O_3 grains, improving the density, physical properties, and fracture toughness of ZTA composites. Naga et al. [15] reported that increasing the Ta_2O_5 concentration can markedly increase the densification and mechanical performance of ZTA ceramics. Arab et al. [16] reported that the formation of the $SrAl_{12}O_{19}$ phase after the addition of $SrCO_3$ to ZTA can improve the fracture toughness; however, this was accompanied by increased porosity. Fracture toughness values of the samples were improved, but the dynamic strength was not enhanced because of the increase in porosity.

Spark plasma sintering (SPS) technology has been used to prepare ceramic composites owing to its fast heating, energy efficiency, and high sintering density [17–20]. SPS can significantly enhance the density, inhibit the growth of Al_2O_3 grains, and promote the t–m transformation toughening of ZrO_2 under external pressure [8, 21].

Although research on ZTA toughening has received widespread attention, there are few studies on the influence of the addition of Nb_2O_5 to ZTA–TiO_2 ceramics prepared by using SPS. Thus, the effect of the amount of added Nb_2O_5 on the phase composition, microstructure, and mechanical performance of ZTA–3TiO_2 composites was studied, and the influence mechanism was analysed.

Experimental procedure

Raw materials

The raw materials used in this paper were Al_2O_3 powder of 0.2 μm (99.99% purity, Aladdin), ZrO_2 (YSZ) powder of 0.1–0.2 μm ($ZrO_2 \geq 94\%$, Guangdong Orient Zirconic Ind Sci & Tech Co., Ltd.), Nb_2O_5 powder with an average diameter of 50 nm (99.90% purity, Aladdin), TiO_2 powder of 0.2–0.4 μm (EP, Aladdin). These powders were used to prepare six types of composite mixtures. Chemical compositions of the six ZTA–3TiO_2–$x$$Nb_2O_5$ (x = 0, 0.25, 0.50, 0.75, 1.00, 1.25 wt.%) powder mixtures are shown in Table 1. The ratio of Al_2O_3 to ZrO_2 was 4:1 (wt.%) in all the powder mixtures [22, 23].

Methods of preparation

Each powder mixture was ball-milled in ethanol with a zirconia ball (diameter: 5 mm) at 300 r/min for 6 h to ensure uniform powder doping. The mass ratio of the grinding ball to the mixed powder was 3:1. The ethanol in the composite slurry was evaporated until the mixture was dry; then, the mixture was completely dried in a dry oven for 12 h. The dried powder was ground and passed through a 0.048 mm aperture sieve. The sieved powder was formed into discs with diameters of 13 mm using the SPS method (SPS 632Lx, Japan). The main parameters for SPS preparation were a pressure of 40 MPa, sintering temperature of 1500 °C, and holding time of 20 min.

Table 1 The composition of the six groups of ZTA–3TiO_2–$x$$Nb_2O_5$ in weight percentage (wt.%)

Number	Sample	ZTA	TiO_2	Nb_2O_5
ZTA-0	ZTA–3TiO_2–0Nb_2O_5	97.00	3	0
ZTA-1	ZTA–3TiO_2–0.25Nb_2O_5	96.75	3	0.25
ZTA-2	ZTA–3TiO_2–0.50Nb_2O_5	96.50	3	0.50
ZTA-3	ZTA–3TiO_2–0.75Nb_2O_5	96.25	3	0.75
ZTA-4	ZTA–3TiO_2–1.00Nb_2O_5	96.00	3	1.00
ZTA-5	ZTA–3TiO_2–1.25Nb_2O_5	95.75	3	1.25

The sintered green bodies were decarburised and thermally etched at 1300 °C for 2 h.

Samples characterizations

The sintered specimens were then ground and polished. X-ray diffraction (XRD, Mini Flex 600) was used to identify the phases in the composites. The 2θ range was 10°–90°, and the scan rate was 5°/min. Microstructures of the composites were observed using scanning electron microscopy (SEM, Zeiss, EVO 180). Energy-dispersive x-ray spectroscopy (EDS, Bruker, XFlash Detector 6-30) was used to analyse the elemental distributions and chemical compositions of the phases. Image Pro software was used to measure the average grain size from the SEM images. Bulk densities of the sintered samples were measured using Archimedes' method, and relative density was defined as the ratio of bulk density to theoretical density. The hardness was measured using the Vickers hardness method (HSV-20, Japan) with a load of 5 kgf; the pressure was maintained for 15 s. The indentation fracture toughness of the composite can be calculated using the crack produced by Vickers indentation, and the Eq. (1) [24] is used to obtain the indentation fracture toughness of the composite.

$$3K_{IC} = 0.035\left(Ha^{0.5}\right)(3E/H)^{0.4}(l/a)^{-0.5} \quad (1)$$

where, K_{IC} is the indentation fracture toughness, H is the Vickers hardness, a is half of the Vickers diagonal indentation, E is Young's modulus, and l is the length of the radial crack.

Results and discussion

Phase composition and Microstructure

Figure 1 shows the XRD patterns of the samples with different Nb_2O_5 contents. Two main diffraction peaks were identified: Al_2O_3 (corundum) and yttria-doped t-ZrO_2 (YSZ). Owing to the addition of TiO_2, weak diffraction peaks of the trace Al_2TiO_5 phase were also present in the patterns. Wang et al. [25] reported that the addition of 3 wt.% TiO_2 to a ZTA composite will result in the formation of Al_2TiO_5. With the addition of Nb_2O_5, the diffraction peaks of the m-ZrO_2 phase appeared. The percentage of t-ZrO_2 and m-ZrO_2 for each sample were calculated by XRD. With the

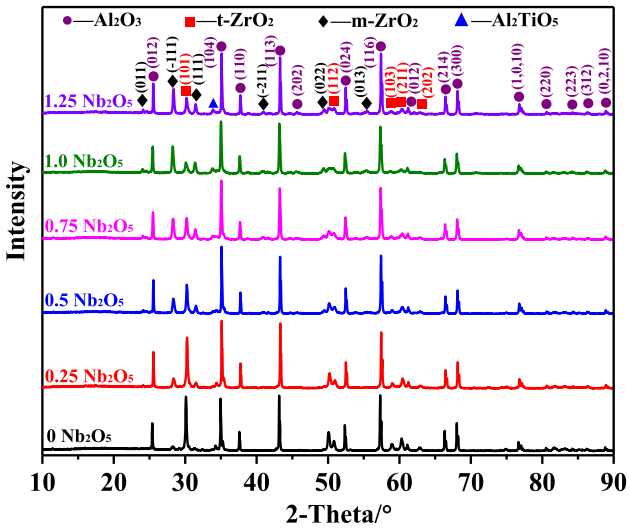

Figure 1 XRD patterns of ZTA–3TiO_2 composites with different Nb_2O_5 contents.

addition of Nb_2O_5 increasing from 0 to 1.25 wt.%, the mass fractions of m-ZrO_2 are 0.6%, 1.9%, 3.5%, 5.4%, 7.4% and 7.5%, while the mass fractions of t-ZrO_2 are 10.7%, 9.6%, 5.3%, 4.2%, 2.1% and 2.2%.

The appearance of the m-ZrO_2 diffraction peaks in the sample without Nb_2O_5 was due to the t–m transformation during the decarburisation and thermal etching processes. Because of the pressure applied during SPS, the samples had a high internal stress. In the subsequent thermal etching process, stress release at high temperatures caused t–m transformation of the ZrO_2 phase. When the Nb_2O_5 content increased to 0.5 wt.%, the (101) diffraction peak of t-ZrO_2 weakened and shifted to a higher diffraction angle; in addition, intensities of the (− 111) and (111) diffraction peaks of m-ZrO_2 increased. When the Nb_2O_5 content is low, Ti atoms partially replace Zr and Y atoms in ZrO_2. Because the radius of Ti atoms is smaller than those of Zr and Y, the lattice parameters are reduced, and the diffraction peaks shift to a higher angle. When the Nb_2O_5 content increased to 1.25 wt.%, the (101) diffraction peak gradually shifted to a lower diffraction angle. The formation of an interstitial solid solution of Nb atoms in the t-ZrO_2 crystal interstices caused the t-ZrO_2 lattice to distort, and the lattice parameters to increase; as a result, the diffraction peak shifted to a lower angle. There were multiple m-ZrO_2 diffraction peaks with different intensities, and the intensities of the (− 111) and (111) diffraction peaks of m-ZrO_2 increased significantly. Schmitt-Radloff et al. [26]

reported that with increases in the sintering temperature and grain size, proportion of the m-ZrO_2 phase increases during the sintering process; therefore, the t–m transformation occurs more easily during the cooling process.

EDS was used to analyse the elemental distributions and chemical compositions of the phases in the sintered samples. Figure 2 shows an SEM backscattered electron image and EDS analysis of the ZTA–$3TiO_2$–$0.75Nb_2O_5$ composite. The grey–black structure mainly contained Al, indicating that it was Al_2O_3; the white structure mainly contained Zr, indicating that it was ZrO_2 (YSZ). In addition, Ti and Nb were significantly enriched in the ZrO_2 grains. Semi-quantitative analysis of the elemental compositions of the phases were conducted using EDS spot scanning. Figure 2b shows the EDS spot scanning results of the white ZrO_2 phase. Combined with the XRD analysis, it can be proved that the white structure was a complex phase comprising a ZrO_2 solid solution containing Ti and Nb atoms and Al_2TiO_5 phases. Phases with special morphologies were not found in the composite microstructure, such as those often found for Al_2TiO_5 and other trace phases. The relative content of the trace phase was small, and the trace phases were attached to the surfaces of the ZrO_2 grains. The external pressure during SPS inhibited the independent growth of the trace phase; therefore, there was no noticeable abnormality in the microstructure.

Figure 3 shows SEM images of the microstructures of the ZTA–$3TiO_2$ samples with different Nb_2O_5 contents. Al_2O_3 grains in the composite existed in the form of equiaxed particles, but the grain size was non-uniform. Compared with traditional pressureless sintering, ZrO_2 grains existed in two forms: block and layered stacking, which are marked with a red solid line and a green-dotted line, respectively. The morphology of the partial ZrO_2 grains transformed from equiaxed particles to irregular shapes, mostly at the Al_2O_3 grain boundaries. In addition, holes with different numbers and sizes existed on the samples with different Nb_2O_5 contents. As the amount of Nb_2O_5 increased, the number and diameter of the holes first decreased and then increased. The number and size of holes in the sample with the largest amount of Nb_2O_5 (1.25 wt.%) were lower than those in the sample without Nb_2O_5.

The effects of Nb_2O_5 on the Al_2O_3 and ZrO_2 grain sizes were analysed, the average grain sizes of the samples with different Nb_2O_5 contents were measured, and the grain size distributions were calculated (Figs. 4, 5). When a small amount of Nb_2O_5 (0.25 wt.%) was added, the grain size of Al_2O_3 was slightly reduced compared with that of the composite without Nb_2O_5, reaching a minimum value of

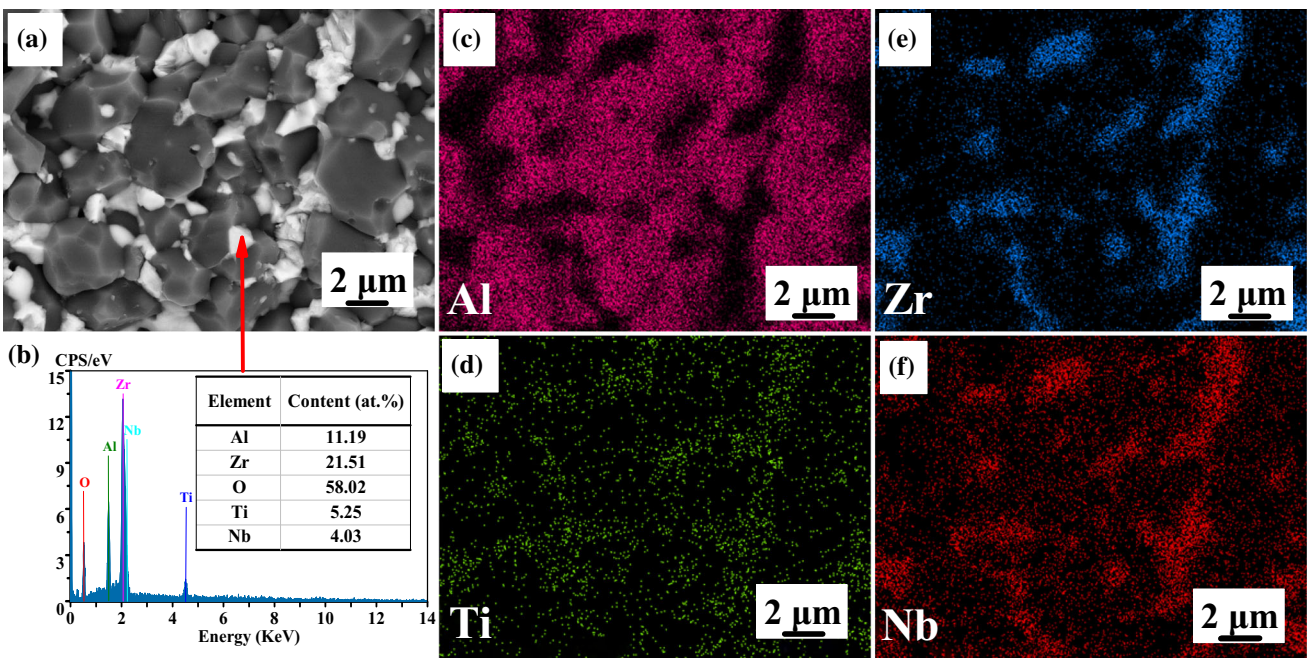

Figure 2 EDS results of ZTA–$3TiO_2$–$0.75Nb_2O_5$ composite.

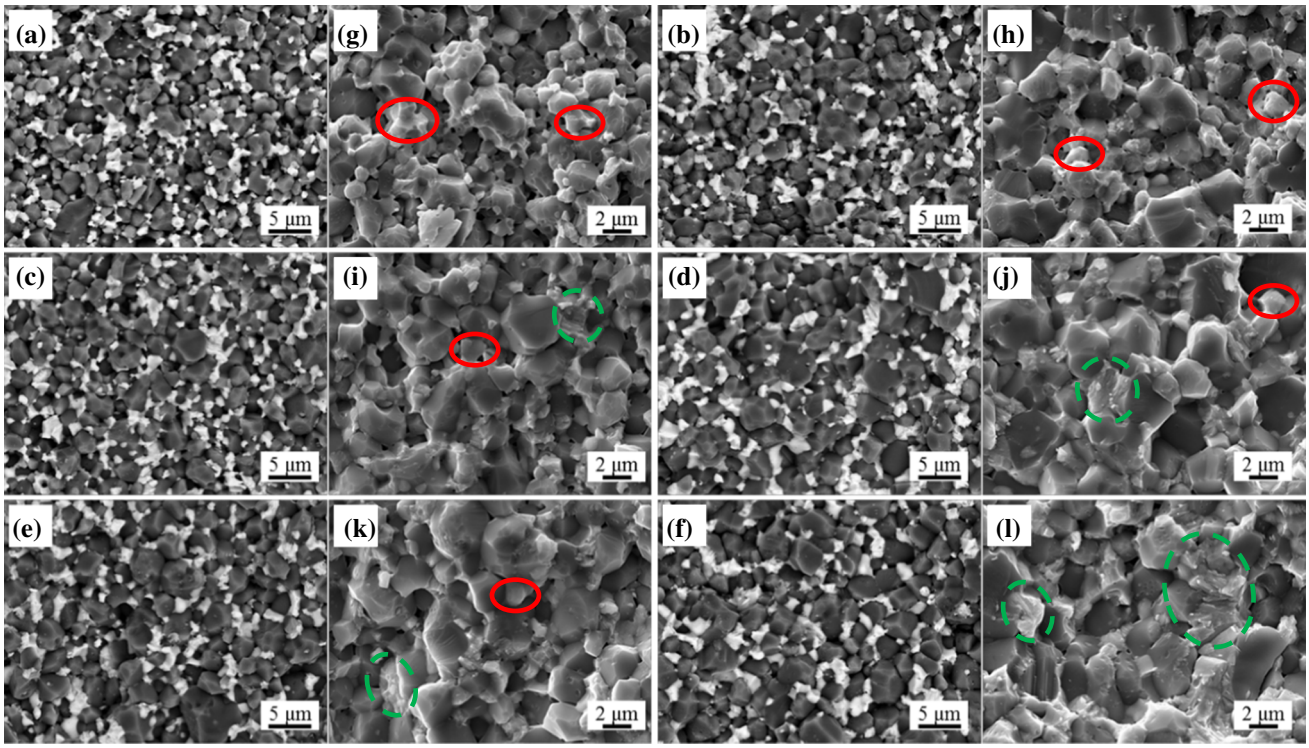

Figure 3 Microstructure and typical fracture surface microstructure of ZTA–3TiO_2 composites with different Nb_2O_5 contents (wt.%): **a**, **g** 0 Nb_2O_5; **b**, **h** 0.25 Nb_2O_5; **c**, **i** 0.50 Nb_2O_5; **d**, **j** 0.75 Nb_2O_5; **e**, **k** 1.0 Nb_2O_5; **f**, **l** 1.25 Nb_2O_5.

2.03 μm. The proportion of grains 1–2 μm in size increased to 57%, and the grain uniformity increased. When the amount of added Nb_2O_5 was > 0.25 wt.%, the size of the Al_2O_3 grains increased significantly; moreover, the uniformity of the grains gradually decreased, and the number of abnormally coarse grains (4–6 μm) increased. When Nb_2O_5 content was 1.25 wt.%, Al_2O_3 grain size reached the maximum value of 2.80 μm. When Nb_2O_5 content was > 0.5 wt.%, Al_2O_3 grain size distribution showed excellent stability, and the proportions of grains in different size ranges remained relatively constant. Seong et al. [27] reported that the addition of Nb_2O_5 can lead to the growth of Al_2O_3 grains, and the optimal amount to be added was similar to that in this study. Notably, the addition of Nb_2O_5 caused a slight increase in the grain size of ZrO_2; the morphology and grain size distribution of ZrO_2 did not change markedly, and the grain size distribution was relatively stable. When Nb_2O_5 content was low, the ZrO_2 grains agglomerated in a lamellar structure; as Nb_2O_5 content gradually increased, the grains transformed into a clumpy morphology. The ZrO_2 grains mainly existed at the grain boundaries of Al_2O_3, and the stress of the SPS method restricted the free flow and diffusion of the high-temperature liquid [28]. This resulted in the rapid and natural nucleation and growth of ZrO_2 grains during the cooling process, and the ZrO_2 grains were deformed under stress. Therefore, the grain size was fine, and there was a lamellar packing morphology.

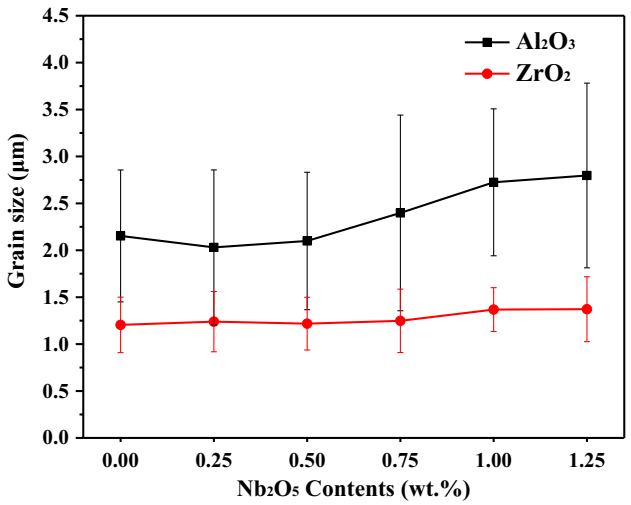

Figure 4 Average grains size of Al_2O_3 and ZrO_2 grains for ZTA–3TiO_2 composites with different Nb_2O_5 contents.

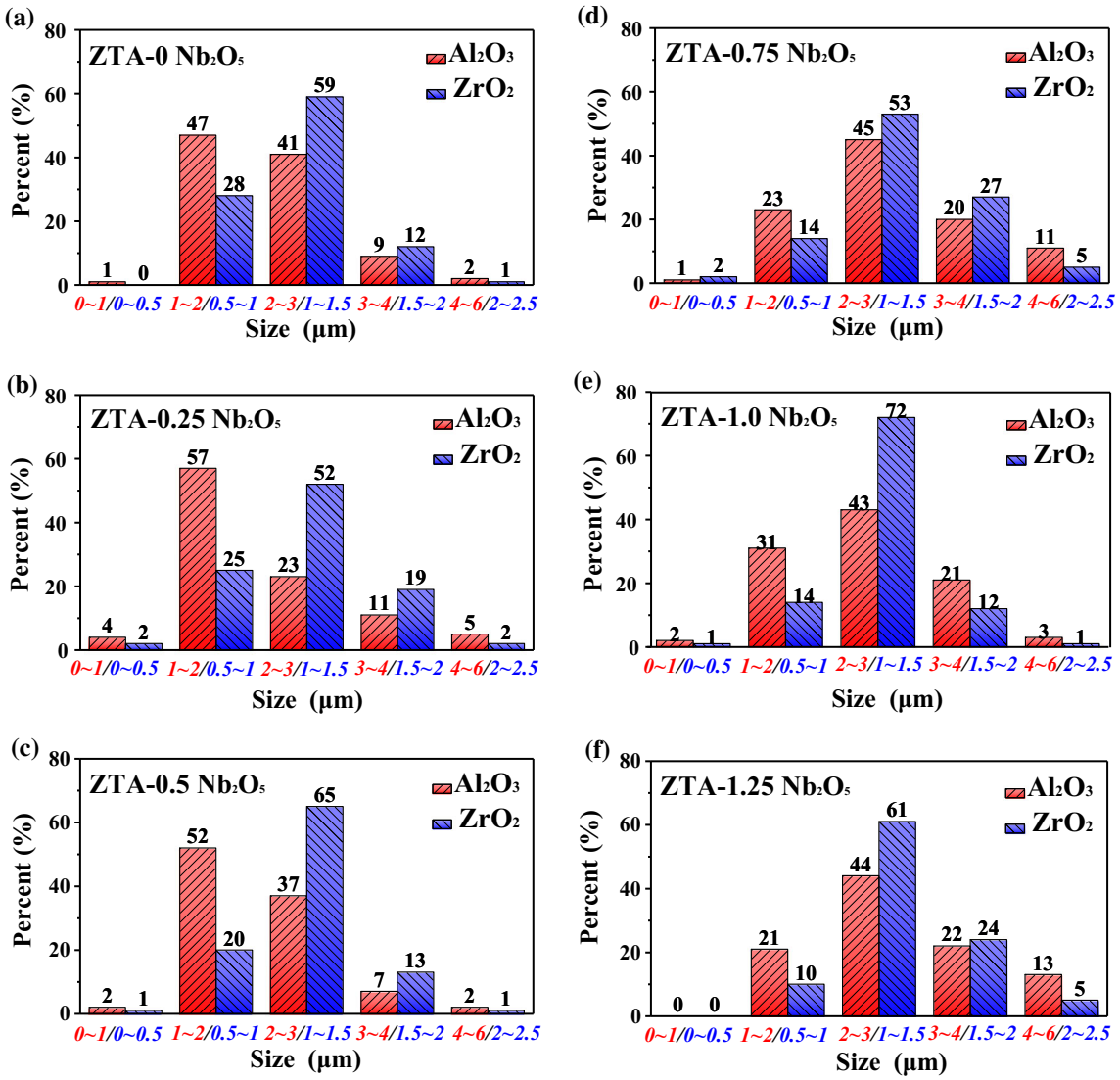

Figure 5 Grain size distribution of Al_2O_3 and ZrO_2 grains for ZTA–3TiO_2 composites with different Nb_2O_5 contents.

Physical and mechanical properties

Figure 6 shows the bulk densities and relative densities of the samples with different amounts of Nb_2O_5. The measured bulk densities and relative densities of the composites were significantly affected by the Nb_2O_5 content. Theoretical densities of the composites with different Nb_2O_5 contents were approximately equal, and the slope of the theoretical density vs. Nb_2O_5 content curve was close to zero; thus, the bulk density and relative density varied in a similar manner. Overall, the bulk density first increased and then decreased with increasing Nb_2O_5 content. Bulk density improved from a minimum value of 4.07 g/cm^3 for the sample without Nb_2O_5 to

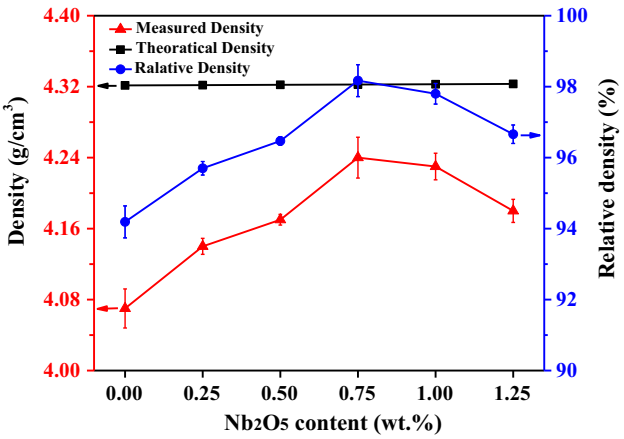

Figure 6 Results of bulk density and relative density of ZTA–3TiO_2 composites with different Nb_2O_5 contents.

a maximum value of 4.24 g/cm^3 for the sample with 0.75 wt.% Nb_2O_5. Correspondingly, relative density of the composite also increased from 94.19 to 98.17%, which is an increase of 4.23%. It is worth noting that the bulk density of the sample with 1.25 wt.% Nb_2O_5 was 4.18 g/cm^3, with relative density decreased by 96.66%; however, it was still higher than that of the sample without Nb_2O_5. The variation in the density matches well the number and size of holes in the microstructure. Interestingly, it does not completely follow the variation in the grain size. In theory, it is easier to obtain a higher density with finer grains. While the sample with 0.25 wt.% Nb_2O_5 had the smallest grain size (2.03 μm), it did not have the maximum density (95.70%). The addition of TiO_2 and trace Nb_2O_5 effectively refined the grains, while excessive Nb_2O_5 increased the Al_2O_3 grain size; however, the grain size was more uniform (Fig. 5). Therefore, grains of uniform size are more conducive to obtaining a dense microstructure.

The Vickers hardness values of the ZTA–3TiO_2 composites with different Nb_2O_5 contents are shown in Fig. 7. The variation in the Vickers hardness with the Nb_2O_5 content can be divided into three stages: it increased first, then decreased slowly, and finally, decreased sharply. The Vickers hardness of the sample with 0.25 wt.% Nb_2O_5 had the maximum value of 1228.40 HV, which was 12.08% higher than that of the sample without Nb_2O_5 (1096.0 HV). When Nb_2O_5 content was > 0.25 wt.%, Vickers hardness gradually decreased. As Nb_2O_5 content increased from 0.25 to 0.75 wt.%, the Vickers hardness decreased by 3.96% from 1228.40 to 1179.80 HV. When Nb_2O_5 content was > 1.0 wt.%, Vickers hardness was significantly reduced. The sample with 1.25 wt.% Nb_2O_5 had the smallest Vickers hardness (957 HV), which was lower than that of the sample without Nb_2O_5.

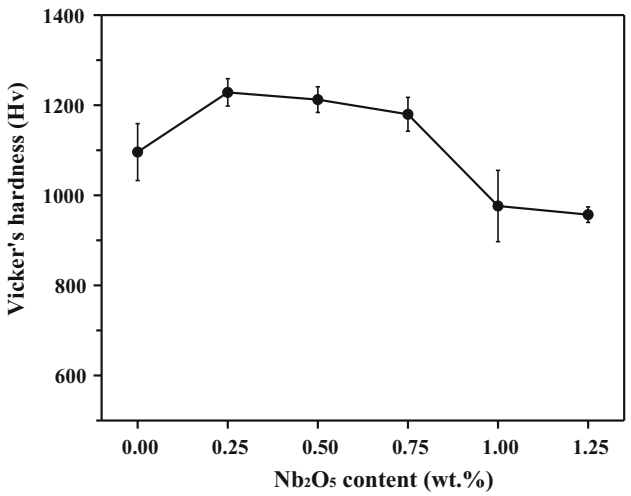

Figure 7 Results of Vickers hardness of ZTA–3TiO_2 composites with different Nb_2O_5 contents.

The change in Vickers hardness was due to the effects of Nb_2O_5 on the grain sizes and relative densities of the samples. The enhancement in Vickers hardness was due to the synergistic effect of grain refinement and increased relative density [29]. Moreover, the fine grains improved the relative density and reduced the porosity and hole size. The hardness of a ceramic can be used to characterise its compressive strength, and the Ryskewitch equation represents the relationship between the strength and porosity of a material, which is given in Eq. (2) [30]:

$$\sigma = \sigma_0 \exp(-aP) \quad (2)$$

where a is the porosity, σ_0 is the strength at which the porosity is zero, and P is a constant whose value lies between 4 and 7.

There are two ways in which holes affect the strength of ceramics: by forming stress concentration points and reducing the strength. Cracks tend to form at defects in the internal region or surface of ceramics. Therefore, grain size and porosity have a synergistic effect on the strength of ceramic materials.

Combining the grain size (Fig. 4) and density (Fig. 6) measurements, the variation in the Vickers hardness is closely related to the grain size. The sample with 0.25 wt.% Nb_2O_5 had the largest Vickers hardness and the smallest Al_2O_3 grain size (2.03 μm); however, its relative density (95.70%) was lower than the maximum value. Therefore, at a high density, the beneficial effect of grain refinement is greater than the adverse effect of the increase in the number and size of the holes on the strength [31]. The samples with 1.0 and 1.25 wt.% Nb_2O_5 had grain sizes of 2.72 and 2.79 μm and the lowest Vickers hardness values of 976.20 and 957.0 HV, respectively, which were lower than those of the sample without Nb_2O_5. Grain growth led to a coarser microstructure of the composite, resulting in reduced Vickers hardness. In particular, in the Vickers hardness test, partial indentation of the samples with 1.0 and 1.25 wt.% Nb_2O_5 caused them to collapse and fracture, as shown in Fig. 8, resulting in indentations without a complete shape and clear outline. The grain sizes of these samples were also the largest, and the coarse

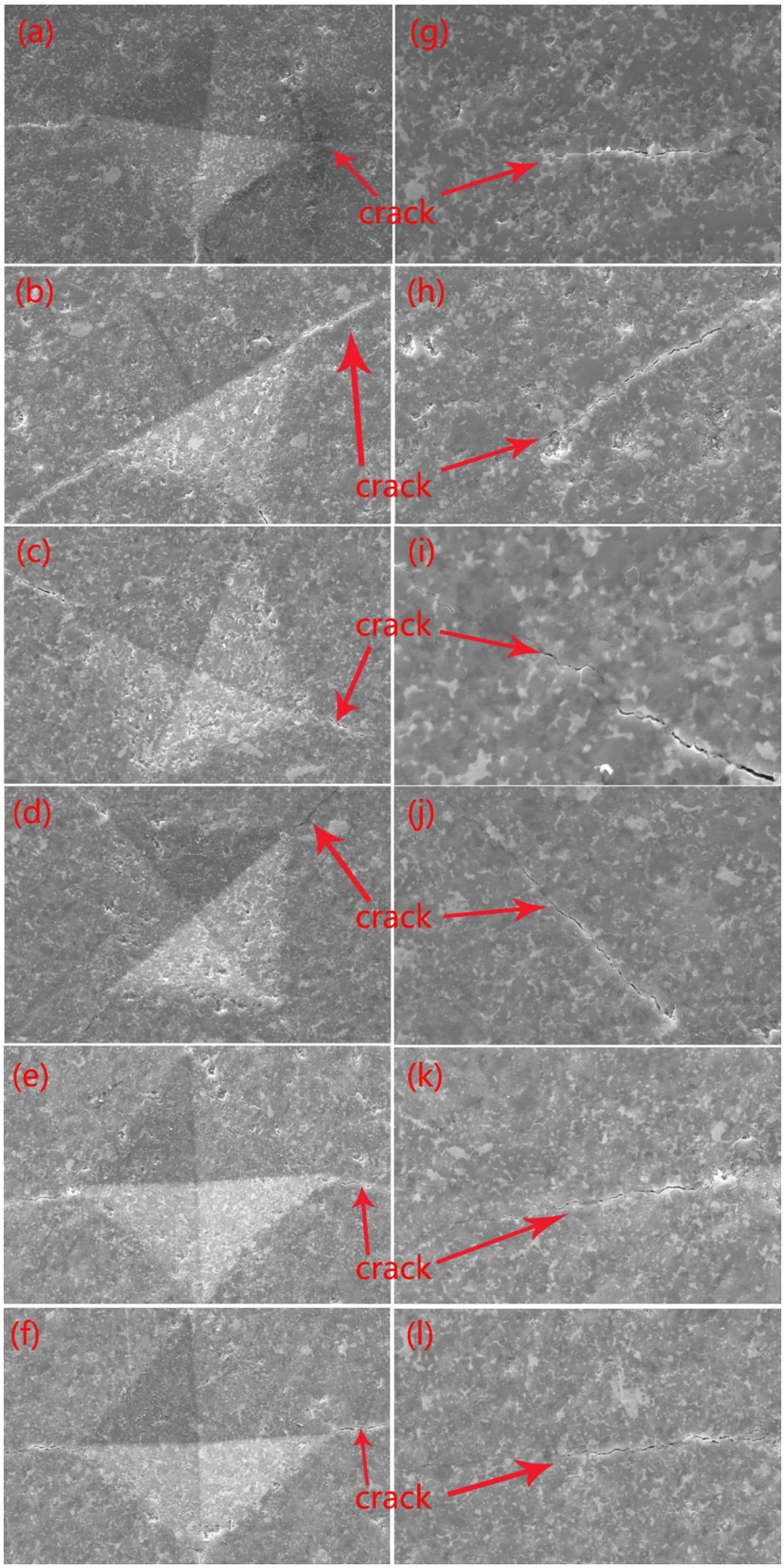

Figure 8 Surface morphology of crack for ZTA–3TiO_2 composite with different Nb_2O_5 content: **a**, **g** 0 Nb_2O_5; **b**, **h** 0.25 Nb_2O_5; **c**, **i** 0.50 Nb_2O_5; **d**, **j** 0.75 Nb_2O_5; **e**, **k** 1.0 Nb_2O_5; **f**, **l** 1.25 Nb_2O_5.

grains had an adverse effect on the density. Therefore, the coarse grains and lower relative densities of the samples with high Nb_2O_5 contents led to a decrease in the strength.

The crack propagation of ZTA–TiO_2–Nb_2O_5 samples with different Nb_2O_5 additives is shown in Fig. 8. Scanning electron microscopy pictures of the indentations display microcracks beginning from the corners of the Vickers indentations. Cracks in all samples were deflected during expansion. Figure 8b shows the crack morphology of the sample with an Nb_2O_5 addition of 0.235 wt.%. Compared with the crack morphology of other samples, the crack has a significant deflection. Moreover, cracks propagate directly through these grains. The crack propagation behaviour indicates that the crack deflection has a toughening effect on the ZTA ceramics, which is also consistent with the fracture toughness results. The reason of the fracture's toughness increasing of the ZTA–Nb_2O_5 ceramics is crack deflection.

Figure 9 shows the indentation fracture toughness of the ZTA–3TiO_2 composites with different amounts of Nb_2O_5. The sample with 0.25 wt.% Nb_2O_5 had the maximum indentation fracture toughness of 9.17 MPa $\sqrt{m}$. As the Nb_2O_5 content increased, the indentation fracture toughness decreased by varying degrees. The indentation fracture toughness of the sample with 1.25 wt.% Nb_2O_5 had the minimum indentation fracture toughness of 7.05 MPa $\sqrt{m}$, which was 23.37% lower than the maximum value. The indentation fracture toughness of the samples with trace amounts of Nb_2O_5 improved mainly

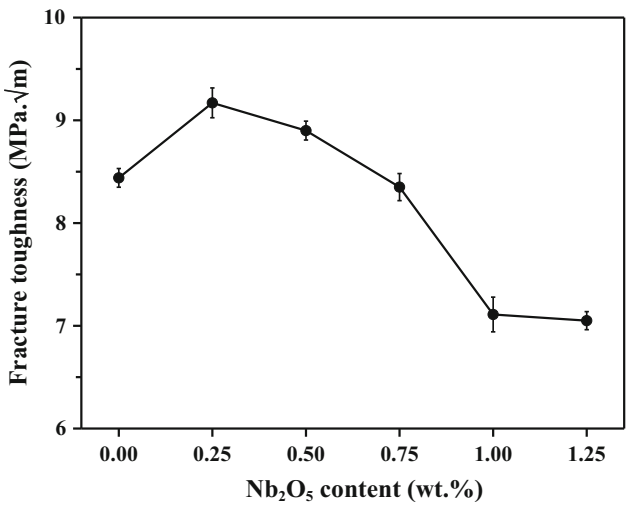

Figure 9 Results of indentation fracture toughness of ZTA–3TiO_2 composites with different Nb_2O_5 contents.

because the addition of TiO_2 and Nb_2O_5 refined the Al_2O_3 grains and suppressed the t–m transformation of t-ZrO_2. At high densities, the addition of TiO_2 and Nb_2O_5 prevents grain growth, and TiO_2, as an YSZ stabiliser, inhibits the t–m transformation of the ZrO_2 phase. In addition, the stress of SPS also inhibits grain growth and the t–m phase transition by limiting the volume expansion. The reduction in the grain size significantly enhanced the strength and toughness of the composites and increased the load-bearing capacity. The suppression of the t–m transformation can promote stress-induced transformation toughening of the t-ZrO_2 phase at room temperature. Adding excessive Nb_2O_5 led to the growth of Al_2O_3 grains, and the metastable t-ZrO_2 underwent t–m transformation, which reduced the phase transformation toughening effect, thereby reducing the indentation fracture toughness.

Conclusions

The effects of Nb_2O_5 content on the microstructure and mechanical performance of ZTA–3TiO_2 composites prepared by SPS were studied. The main research conclusions are as follows:

1. The addition of TiO_2 stabilises the metastable t-ZrO_2, inhibits the ZrO_2 transformation, and generates Al_2TiO_5 phase. The addition of trace Nb_2O_5 does not produce a new niobium-rich phase, and Nb atoms are dissolved in ZrO_2 grains. But, the addition of excessive Nb_2O_5 promotes the t-m transformation of the t-ZrO_2 phase producing the m-ZrO_2.
2. When the content of Nb_2O_5 is less than 0.25 wt.%, TiO_2 and Nb_2O_5 inhibit the grain growth of Al_2O_3 and ZrO_2. When the contents of Nb_2O_5 exceed 0.25 wt.%, partly TiO_2 stabilizer is replaced by Nb_2O_5, which reduces the ability of TiO_2 on grain refinement. However, the addition of Nb_2O_5 promotes the stability of grains size and improves the uniformity of the microstructure.
3. The density of ZTA–3TiO_2 composite gradually improves with the increase of Nb_2O_5 content, the sample with 0.75 wt.% Nb_2O_5 shows the maximum relative density of 98.17%. As the Nb_2O_5 content increases to 1.25 wt.%, the density decreases, but the density higher than the sample

without Nb_2O_5. The grain size of the sample with 0.25 wt.% Nb_2O_5 is the smaller of 2.03 μm.

4. When Nb_2O_5 content is 0.25 wt.%, the Vickers hardness and indentation fracture toughness reach the maximum value, which are 1228.40 HV and 9.17 MPa $\sqrt{m}$, respectively. However, as the addition amount of Nb_2O_5 further increases, the grains growth and the decrease in relative density result in a reduction in Vickers hardness and indentation fracture toughness. Therefore, in the case of high relative density, the grain size plays a decisive role in the mechanical properties of the composite.

Funding

This study was funded by National Natural Science Foundation of China (grant number 52265022).

Declarations

Conflict of interest The authors declare that they have no conflict of interest.

References

[1] Basha MM, Basha SM, Singh BK, Mandal N, Sankar MR (2020) A review on synthesis of zirconia toughened alumina (ZTA) for cutting tool applications. Mater Today Proc 26:534–541

[2] Fan JY, Lin TT, Hu FX, Yu Y, Ibrahim M, Zheng RB, Huang SB, Ma JF (2017) Effect of sintering temperature on microstructure and mechanical properties of zirconia-toughened alumina machinable dental ceramics. Ceram Int 43:3647–3653

[3] Sarkar M, Sadhu KK, Chakraborty SS, Mandal N (2022) Simultaneous effect of CaF_2 and TiC on tribological properties of ZTA ceramics for high temperature application. Mater Today Proc 57:116–120

[4] Sktani ZDI, Rejab NA, Rosli AFZ, Arab A, Ahmad ZA (2021) Effects of La_2O_3 addition on microstructure development and physical properties of harder ZTA–CeO_2 composites with sustainable high fracture toughness. J Rare Earth 39:844–849

[5] Kelly PM, Rose LRF (2002) The martensitic transformation in ceramics—its role in transformation toughening. Prog Mater Sci 47:463–557

[6] Chevalier J, Gremillard L, Virkar AV, Clarke DR (2009) The tetragonal-monoclinic transformation in zirconia: lessons learned and future trends. J Am Ceram Soc 92:1901–1920

[7] Rejab NA, Azhar AZA, Ratnam MM, Ahmad ZA (2013) The relationship between microstructure and fracture toughness of zirconia toughened alumina (ZTA) added with MgO and CeO_2. Int J Refract Met Hard Mater 41:522–530

[8] Akin I, Yilmaz E, Ormanci O, Sahin F, Yucel O, Goller G (2010) Effect of TiO_2 addition on the properties of Al_2O_3–ZrO_2 composites prepared by spark plasma sintering. Bioceram Dev Appl 1:1–3

[9] Tan P, Yang Y, Sui YD, Jiang YH (2020) Influence of CeO_2 addition on the microstructure and mechanical properties of zirconia-toughened alumina (ZTA) composite prepared by spark plasma sintering. Ceram Int 46:7510–7516

[10] Manshor H, Aris SM, Azhar AZA, Abdullah EC, Ahmad ZA (2015) Effects of TiO_2 addition on the phase, mechanical properties, and microstructure of zirconia-toughened alumina ceramic composite. Ceram Int 41:3961–3967

[11] Sktani ZDI, Arab A, Mohamed JJ, Ahmad ZA (2022) Effects of additives additions and sintering techniques on the microstructure and mechanical properties of zirconia toughened alumina (ZTA): a review. Int J Refract Met Hard Mater 106:105870. https://doi.org/10.1016/j.ijrmhm.2022.105870

[12] Guo L, Li M, Ye F (2016) Phase stability and thermal conductivity of RE_2O_3 (RE=La, Nd, Gd, Yb) and Yb_2O_3 co-doped Y_2O_3 stabilized ZrO_2 ceramics. Ceram Int 42:7360–7365

[13] Xia J-F, Nian H-Q, Liu W, Wang X-G, Jiang D-Y (2016) Effect of Cr_2O_3 derived from $Cr(NO_3)_3{\cdot}9H_2O$ precursor on the densification and mechanical properties of zirconia-toughened alumina (ZTA) composites. Ceram Int 42:9116–9124

[14] Sui YD, Han LN, Jiang YH (2018) Effect of Ta_2O_5 addition on the microstructure and mechanical properties of TiO_2-added yttria-stabilized zirconia-toughened alumina (ZTA) composites. Ceram Int 44:14811–14816

[15] Naga SM, Hassan AM, Awaad M (2015) Physical and mechanical properties of Ta_2O_5 doped zirconia-toughened alumina (ZTA) composites. Ceram Int 41:6248–6255

[16] Arab A, Ahmad R, Ahmad ZA (2016) Effect of $SrCO_3$ addition on the dynamic compressive strength of ZTA. Int J Miner Metall Mater 23:481–489

[17] Meena KL, Karunakar DB (2018) Development of alumina toughened zirconia nanocomposites using spark plasma sintering. Mater Today Proc 5:16928–16935

[18] Haji Seyedrazi SS, Taheri-Nassaj E (2018) Effects of Y_2O_3 additive percentage on MgO ceramic by co-precipitation and SPS methods. Mater Chem Phys 219:96–108

[19] Lallemant L, Roussel N, Fantozzi G, Garnier V, Bonnefont G, Douillard T, Durand B, Guillemet-Fritsch S, Chane-Ching JY, Garcia-Gutierez D, Aguilar-Garib J (2014) Effect of amount of doping agent on sintering, microstructure and optical properties of Zr- and La-doped alumina sintered by SPS. J Eur Ceram Soc 34:1279–1288

[20] Peng ZJ, Luo XD, Xie ZP, Yang MM (2019) Sintering behavior and mechanical properties of spark plasma sintering SiO_2–MgO ceramics. Ceram Int 46:2585–2591

[21] Chakravarty D, Sundararajan G (2013) Microstructure, mechanical properties and machining performance of spark plasma sintered Al_2O_3–ZrO_2–TiCN nanocomposites. J Eur Ceram Soc 33:2597–2607

[22] Azhar AZA, Shawal SHM, Manshor H, Ali AM, Rejab NA, Abdullah EC, Ahmad ZA (2019) The effects of CeO_2 addition on the physical and microstructural properties of ZTA–TiO_2 ceramics composite. J Alloys Compd 773:27–33

[23] Chen J, Xie Z, Zeng W, Wu W (2017) Toughening mechanisms of ZTA ceramics at cryogenic temperature (77K). Ceram Int 43:3970–3974

[24] Exare C, Kiat JM, Guiblin N, Porcher F, Petricek V (2015) Structural evolution of ZTA composites during synthesis and processing. J Eur Ceram Soc 35:1273–1283

[25] Wang C-J, Huang C-Y (2008) Effect of TiO_2 addition on the sintering behavior, hardness and fracture toughness of an ultrafine alumina. Mater Sci Eng A 492:306–310

[26] Schmitt-Radloff U, Kern F, Gadow R (2018) Spark plasma sintering and hot pressing of ZTA–NbC materials—a comparison of mechanical and electrical properties. J Eur Ceram Soc 38:4003–4013

[27] Seong WK, Ahn BM, Min YH, Hwang GT, Choi JJ, Choi JH, Hahn BD, Cho YR, Ahn CW (2020) Effect of Nb_2O_5 addition on microstructure and thermal/mechanical properties in zirconia-toughened alumina sintered at low temperature. Ceram Int 46:23820–23827

[28] Powers JD, Glaeser AM (1998) Grain boundary migration in ceramics. Interface Sci 6:23–39

[29] Garcia RHL, Ussui V, de Lima NB, Muccillo ENS, Lazar DRR (2009) Physical properties of alumina/yttria-stabilized zirconia composites with improved microstructure. J Alloys Compd 486:747–753

[30] Bian HM, Yang Y, Wang Y, Tian W, Jiang HF, Hu ZJ, Yu WM (2013) Effect of microstructure of composite powders on microstructure and properties of microwave sintered alumina matrix ceramics. J Mater Sci Technol 29:429–433

[31] Pereira da Silva JG, Yamchelou AN, Debris A, Wieck C, Jelitto H, Al-Qureshi HA, Janssen R (2017) Mechanical strength and defect distributions in flash sintered 3YSZ. J Eur Ceram Soc 37:2901–2905